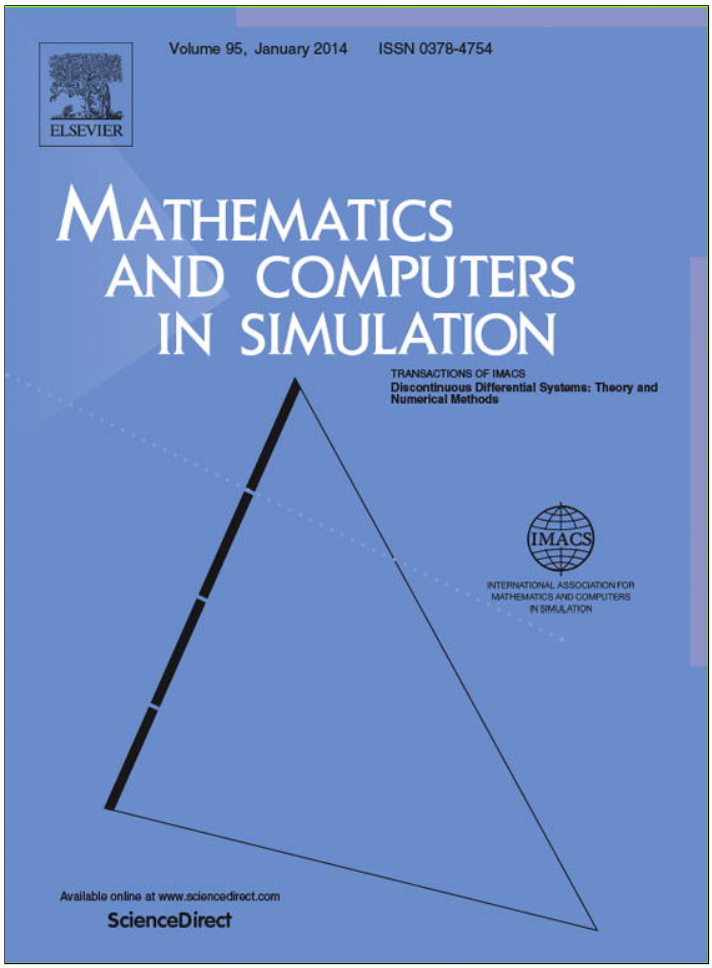

Available online at www.sciencedirect.com

SciVerse ScienceDirect

Mathematics and Computers in Simulation 95 (2013) 78–97

MATHEMATICS AND COMPUTERS IN SIMULATION

www.elsevier.com/locate/matcom

Original article

On the numerical and computational aspects of non-smoothnesses that occur in railway vehicle dynamics

H. True*, A.P. Engsig-Karup, D. Bigoni

DTU Informatics, The Technical University of Denmark, Asmussens Alle 305, DK-2800 Kgs Lyngby, Denmark

Received 1 September 2011; received in revised form 8 August 2012; accepted 28 September 2012
Available online 13 October 2012

Abstract

The paper contains a report of the experiences with numerical analyses of railway vehicle dynamical systems, which all are nonlinear, non-smooth and stiff high-dimensional systems. Some results are shown, but the emphasis is on the numerical methods of solution and lessons learned. But for two examples the dynamical problems are formulated as systems of ordinary differential-algebraic equations due to the geometric constraints. The non-smoothnesses have been neglected, smoothened or entered into the dynamical systems as switching boundaries with relations, which govern the continuation of the solutions across these boundaries. We compare the resulting solutions that are found with the three different strategies of handling the non-smoothnesses. Several integrators – both explicit and implicit ones – have been tested and their performances are evaluated and compared with respect to accuracy, and computation time.

Keywords: Railway vehicle dynamics; Stiff systems; Nonlinear dynamics; Non-smoothness

1. Introduction

In recent years the world has seen a rapid development of theoretical research in the area of non-smooth dynamical systems. This development is a natural extension of the mathematical theory of nonlinear dynamical systems that are assumed 'sufficiently smooth', which usually means that all partial derivatives of second order in the dynamical system must be continuous. The area of mathematical theory of nonlinear sufficiently smooth dynamical systems grew very fast in the 20th century. In the second half of the century the development was strongly fueled by the growing application of digital computers and efficient numerical methods that together made it possible to solve nonlinear dynamical problems that hitherto had not been solvable with the known analytic solution methods.

In real life, however, the dynamical problems often do not satisfy the 'sufficiently smooth' criterion, and many of the mathematical results are not valid any more. Solutions of non-smooth problems were therefore limited in number but of important examples the theory of the clock and the motion of a body under the action of a Coulomb type friction force ought to be mentioned. These dynamical systems were simple one degree of freedom systems. As examples of the breakdown of the mathematical theory for smooth dynamical systems we mention the center manifold theorem for bifurcations and the necessary condition for existence of a bifurcation, which both do not hold in general for

* Corresponding author. Tel.: +45 4525 3016.
E-mail address: ht@imm.dtu.dk (H. True).

0378-4754/$36.00
http://dx.doi.org/10.1016/j.matcom.2012.09.016

non-smooth dynamical systems. Instead numerical continuation routines must be applied to find bifurcation points and multiple attractors. This fact emphasizes the importance of accurate and reliable numerical methods for the analysis of theoretical dynamical problems.

Nonlinear dynamical models of mechanical systems with more than two degrees of freedom (DOF) are in general not solvable by analytic methods, but with the development of the digital computer the impossible became possible, and a vast amount of dynamical models of mechanical systems of interest for the applications could then be analyzed. Vehicle system dynamics is one of such mechanical systems.

Complete dynamical models of vehicle systems are nonlinear and non-smooth with degrees of freedom (DOFs) in the range from about 10 to above 100. It is therefore necessary to find the solutions by numerical methods. In the beginning of the age of numerical investigations of vehicle system dynamics the numerical routines were rather crude, mostly explicit formulations with fixed step length and error tolerance. No special attention was given to the non-smoothnesses in the problem, but they often caused problems of their own. The interest in the numerical methods was limited to the question: Do I get an answer? If 'yes', then fine. An investigation of numerical integration methods for vehicle dynamical problems is found in chapter 2 in the book by Garg and Dukkipatti [7] from 1984. It describes the state of the art at that time. The authors mainly compare explicit and implicit solution routines and show the relative performances of several integration schemes from that time. No attention is paid to the handling of non-smoothnesses in the system.

Around the same time a production of simulation routines for modeling and analysis of vehicle dynamical systems started around the world. New integration routines were developed that were especially designed for vehicle dynamical use. Characteristic for vehicle dynamical systems is the mathematical formulation as a differential-algebraic dynamical problem, which is very stiff. The routine DASSL deserves to be mentioned in this context. Several of these routines are commercially available and have been further developed and used successfully in both industry and research institutes. Some of them participated in a Manchester benchmark test [15] in 1998, where their performances were compared.

In this article we will describe the development of the numerical handling of non-smooth vehicle dynamical systems at The Technical University of Denmark. On the background of some results with bifurcations of as well periodic, quasi-periodic as chaotic solutions and the existence of multiple attractors, we discuss the use of various numerical solution routines. In the long period of applications we have investigated problems with discontinuous second derivatives, discontinuous first derivatives and discontinuous functions. The size of the dynamical problems varies from low-dimensional test problems to high-dimensional realistic railway vehicle models. We have solved these problems as well by ignoring the non-smoothnesses as by smoothing them and by introduction of switching boundaries with event detection. We have compared the solutions that resulted from the various approaches and tried to select a solution strategy that would perform in an optimal way for each given problem. We would like to share our experiences with other members of the scientific and industrial community. In a final section of the article we shall compare the performance of several of the routines we have used and give recommendations for their applications to non-smooth dynamical problems on the basis of our experience.

The reader, who wants information about the general problem of nonlinear railway dynamics, may find [34] a useful reference. An article by Knothe and Böhm [21] describes the history of railway dynamics and both contributions [34,21] contain many references for further studies. The EUROMECH 500 workshop entitled 'Non-smooth Problems in Vehicle Systems Dynamics' was held in 2008, and the contributions are published in the proceedings [32].

A very informative state-of-the art article on numerical methods in vehicle system dynamics by Arnold et al. [1] has recently been published. It is a valuable evaluation and a description of the use of the various available integration routines for vehicle system dynamical problems that exist today.

2. Theoretical basis for railway vehicle dynamical systems

The theoretical model of the dynamics of railway vehicles is usually formulated as a dynamical multibody system under external forcing. The single bodies are most often assumed rigid. Flexible bodies may appear, but the flexibilities are then often represented by a Galerkin approximation of their characteristic frequencies of deformation in order to avoid the modeling of the dynamics of the flexible bodies by partial differential equations. The internal forces between the bodies can be classified in two main groups: (i) spring and damper forces and (ii) contact forces. The spring and damper forces are in general nonlinear, and the contact forces, which always are nonlinear, can be divided into rolling

contact, sliding contact with stick/slip and impacts. All these forces introduce non-smoothnesses in the dynamical system.

The dynamical system depends on several parameters from which the speed, V, is usually chosen as the control parameter in a co-dimension 1 problem. In some applications other control parameters may appear, e.g., in curving, where the radius of the curve and the so-called super elevation, which describes the slope of a cross-section of the track, are important independent parameters. All other parameters are considered constant.

If N is the number of degrees of freedom of the multibody problem with time, t, as the independent variable and $\mathbf{P}$ a set of independent parameters, then we obtain the $2N$ state variables $x_i(t;\mathbf{P})$, $1 \le i \le 2N$, and the dynamical system can be written as a general nonlinear initial value problem on the form

$$\frac{d\mathbf{x}}{dt} = \mathbf{F}(\mathbf{x}, t; \mathbf{P}), \quad t > 0 \tag{1}$$

with appropriate initial conditions $\mathbf{x}(0)$ where M is the number of independent parameters. Thus, $\mathbf{x}(t) \in \mathbb{R}^{2N}$ and $\mathbf{P} \in \mathbf{R}^M$. The vector function $\mathbf{F}(\mathbf{x}, t; \mathbf{P}) \in \mathbb{R}^{2N}$ is a nonlinear and in general a non-smooth function of its arguments.

In addition there are constraint equations. For each wheel set of K total sets an equation of the form

$$\frac{dx_k}{dt} = f_k(\mathbf{x}, t; \mathbf{P}), \quad k = 1, 2, \ldots, K \tag{2}$$

expresses that the two wheels on the axle rotate with the same angular velocity (the axle is assumed rigid) or with different velocities when an elastic connection between the wheels is assumed. The rolling contact parameters of the wheel/rail contact surface are calculated on the basis of the geometrical contours of the two bodies, their relative orientations and the normal load in the contact surface. In real life the relations are non-smooth, and must be evaluated numerically and tabulated. The condition that the wheels and rails are in contact is expressed by a set of constraint equations that combine the kinematic contact variables in a nonlinear relation. These relations together with other possible contact conditions between the bodies in the system constitute a set of constraint equations. These reduce the number of generalized coordinates in the problem to a value below N. Under the influence of dynamical forces on the system some of these relations may become time dependent. The sudden changes in the number of generalized coordinates – for example if a wheel lifts off from the rail – introduces additional non-smoothnesses in the system.

The wheel/rail forces in the rolling contact are explicitly formulated as nonlinear relations between the normal and tangent forces in the contact surface on one side and the deformation under normal load and the normalized accumulated tangential strain velocities in the contact surface – the so-called creepage – on the other. The resulting tangent forces – denoted the creep forces – depend non-linearly on the normal forces, the wheel/rail contact geometry and the creepage. Since the contact surface kinematic relations depend non-smoothly on the relative orientations of the wheel and the rail so do the wheel/rail forces. All non-smoothnesses in the dynamical problem including those that represent sliding contact and impacts should be defined by the switching boundaries $h_j(\mathbf{x}) = 0$, where $1 \le j \le J$, and J is the number of non-smoothnesses with corresponding relations. More about that in Section 5.2.

In this article we mainly consider equilibrium solutions of the dynamical problems, therefore the dynamical systems become autonomous.

The dynamics of a complete wagon model running on straight track or in canted curved tracks can be studied using the Newton–Euler formulation of the dynamical system. Several reference frames are introduced in order to simplify the description of the system:

- the *inertial reference frame I* cannot be used because the model is quickly moving and the dynamics that need to be observed are in the order of the 10^{-3}–10^{-6} m.
- a *track following reference frame F* is attached to the centerline of the track, at the level of the height of the rails, and it moves with the train. This reference frame can be inertial if the track is straight and the train moves at constant speed. Otherwise the frame is not inertial and fictitious forces need to be added to the system.
- each body has its own reference frame, called the *body following reference frame* that is attached to the center of mass of the body.
- additional reference frames, called the *contact point reference frames*, can be used for the modeling of wheel–rail contact forces.

For each body in the system the Newton–Euler relations hold:

$$\sum_{i=1}^{n} {}^{I}\vec{F}_i = m\vec{a} \quad \text{(Newton's law)} \tag{3}$$

$$\sum_{i=1}^{m} {}^{B}\vec{M}_i = \frac{d}{dt}({}^{B}[J]{}^{B}\vec{\omega}) + {}^{B}\vec{\omega} \times ({}^{B}[J]{}^{B}\vec{\omega}) \quad \text{(Euler's law)} \tag{4}$$

where ${}^{I}\vec{F}_i$ and ${}^{B}M_i$ are, respectively, the forces and torques acting on the center of mass, m and $[J]$ are the mass and the tensor moment of inertia respectively, $\vec{a}$ and $\dot{\vec{\omega}}$ are the linear acceleration and the angular acceleration of the bodies. The left superscripts stand for the inertial or the body reference frame. Fictitious forces and torques are added in order to be able to write all the equations of motion in the track following reference frame. The simplification of negligible torque terms leads to the following fictitious forces:

$${}^{F}\vec{F}_c = \begin{Bmatrix} 0 \\ m\left[\dfrac{v^2}{R}\cos(\phi_t)\right] \\ m\left[-\dfrac{v^2}{R}\sin(\phi_t)\right] \end{Bmatrix} \tag{5}$$

where v is the speed of the train, R is the radius and ϕ_t is the cant of the track in the curve and the superscript F indicates that the force is written in the track following reference frame. All the bodies will be subject to the gravitational forces as well:

$${}^{F}\vec{F}_g = \begin{Bmatrix} 0 \\ -mg\,\sin\phi_t \\ -mg\,\cos\phi_t \end{Bmatrix} \tag{6}$$

The contact forces can be split in guidance forces, determined by the normal load and the positive conicity of the wheels, and creep forces, due to the shear and sliding of the wheels on the rails. For the modeling of these forces, several approximations exist, that go from the use of a stiff non-linear spring to the realistic approach to the contact problem. The notation ${}^{F}\vec{F}_{N_l}$ and ${}^{F}\vec{F}_{N_r}$ will be used to refer to the guidance forces on the left and the right wheel of a wheel set. In the same way, the notation ${}^{F}\vec{F}_{C_l}$ and ${}^{F}\vec{F}_{C_r}$ will be used for the creep forces. The total forces on the left and the right wheel of a wheel set will be denoted by ${}^{F}\vec{F}_L$ and ${}^{F}\vec{F}_R$ respectively. The torques due to these forces will also be considered and will be denoted by ${}^{B}\vec{M}_L$ and ${}^{B}\vec{M}_R$.

The last groups of forces that are applied to all the bodies are the suspension forces. Each element of the suspension, generically called *link*, will be characterized by a function f such that

$$\begin{Bmatrix} {}^{F}\vec{F}_l \\ {}^{F}\vec{T}_l \end{Bmatrix} = f({}^{F}\vec{b}_{l_0}, {}^{F}\vec{b}_l, {}^{F}\vec{v}_l, {}^{F}\vec{\theta}_l, {}^{F}\dot{\vec{\theta}}_l) \tag{7}$$

where ${}^{F}\vec{b}_{l_0}$ is the length of the link at rest, ${}^{F}\vec{b}_l$ is the deformed length of the link, ${}^{F}\vec{v}_l$ is the relative speed of the two attack points of the link, ${}^{F}\vec{\theta}_l$ is the deformed angle between the bodies connected by the link and ${}^{F}\dot{\vec{\theta}}_l$ is the angular velocity of the bodies. These quantities can be easily computed using basic geometry, knowing the positions at which the links are connected and the state of the dynamics. The characteristic function of the link, that is usually non-linear, will determine the resulting forces and the torques. Each suspension system is a collection of spring and damping elements. The total resulting forces and torques due to the ith suspension system will be denoted by ${}^{F}\vec{F}_s^i$ and ${}^{B}\vec{M}_s^i$.

Substituting the gravitational, the centrifugal and the suspension forces in (3) and (4), the equation of motion (EOM) of the car body can be obtained.

$$m\ddot{\vec{x}} = {}^{F}\vec{F}_g^C + {}^{F}\vec{F}_c^C + {}^{F}\vec{F}_s^{SS_l} + {}^{F}\vec{F}_s^{SS_t} \tag{8}$$

$$[J]\dot{\vec{\omega}} = {}^{B}\vec{M}_g^C + {}^{B}\vec{M}_c^C + {}^{B}\vec{M}_s^{SS_l} + {}^{B}\vec{M}_s^{SS_t} \tag{9}$$

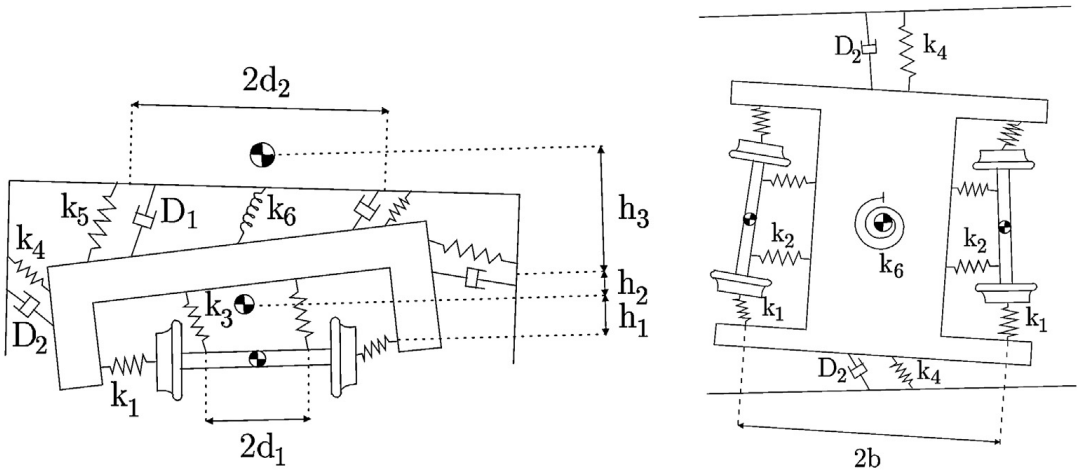

(a) Front view of the bogie (b) Top view of the bogie

Fig. 1. The Cooperrider bogie model.

where the superscript C stands for the car body and $SS_{l/t}$ indicates the leading and trailing secondary suspensions. Similarly, the EOM of the leading bogie frame can be obtained:

$$m\ddot{\vec{x}} = {}^{F}\vec{F}_g^{B_l} + {}^{F}\vec{F}_c^{B_l} + {}^{F}\vec{F}_s^{SS_l} + {}^{F}\vec{F}_s^{PS_{ll}} + {}^{F}\vec{F}_s^{PS_{lt}} \tag{10}$$

$$[J]\dot{\vec{\omega}} = {}^{B}\vec{M}_g^{B_l} + {}^{B}\vec{M}_c^{B_l} + {}^{B}\vec{M}_s^{SS_l} + {}^{B}\vec{M}_s^{PS_{ll}} + {}^{B}\vec{M}_s^{PS_{lt}} \tag{11}$$

where B stands for the leading bogie frame and $PS_{ll/lt}$ indicate, respectively, the leading and trailing primary suspensions. A similar notation is used for the trailing bogie frame. Since the wheel sets are spinning on the track, the pitch angle is not relevant. However, the angular velocity is important in the computation of the creepages as it is given by the nominal spinning speed $\frac{v}{r_0}$ and the speed perturbation β due to the odd distribution of the forces among the wheels. The resulting equations of motion for the leading wheel set attached to the leading bogie frame can be written as:

$$m\ddot{\vec{x}} = {}^{F}\vec{F}_g^{W_{ll}} + {}^{F}\vec{F}_c^{W_{ll}} + {}^{F}\vec{F}_L^{W_{ll}} + {}^{F}\vec{F}_R^{W_{ll}} + {}^{F}\vec{F}_s^{PS_{ll}} \tag{12}$$

$$\begin{aligned} J_\phi\ddot{\phi} = {} & \left\{{}^{B}M_L^{W_{ll}}\right\}_\phi + \left\{{}^{B}M_R^{W_{ll}}\right\}_\phi \\ & + \left\{{}^{B}\vec{M}_g^{W_{ll}}\right\}_\phi + \left\{{}^{B}\vec{M}_c^{W_{ll}}\right\}_\phi + \left\{{}^{B}\vec{M}_s^{PS_{ll}}\right\}_\phi \end{aligned} \tag{13}$$

$$J_\chi\dot{\beta} = \left\{{}^{B}M_L^{W_{ll}}\right\}_\chi + \left\{{}^{B}M_R^{W_{ll}}\right\}_\chi \tag{14}$$

$$\begin{aligned} J_\psi\ddot{\psi} = {} & \left\{{}^{B}M_L^{W_{ll}}\right\}_\psi + \left\{{}^{B}M_R^{W_{ll}}\right\}_\psi \\ & + \left\{{}^{B}\vec{M}_g^{W_{ll}}\right\}_\psi + \left\{{}^{B}\vec{M}_c^{W_{ll}}\right\}_\psi + \left\{{}^{B}\vec{M}_s^{PS_{ll}}\right\}_\psi \end{aligned} \tag{15}$$

where W stands for wheel set and the resulting forces are given by the sum of gravitational, centrifugal, suspension and contact forces. The notation $\{\vec{a}\}_i$ stands for the ith component of the vector $\vec{a}$. Similar equations can be derived for the remaining wheel sets of the model.

Depending on the level of accuracy that is wanted, assumptions can be made in order to simplify the model. For example the car body could be considered fixed if only the dynamics of the wheel sets and the bogie frames need to be analyzed.

3. Models with impact

The dynamics of Cooperrider's bogie model [4] has been investigated in detail. The model is shown in Fig. 1. A detailed description of the model is presented by Kaas-Petersen in [17] (notice a printing error on p. 92. G is correctly 8.08×10^{10} N/m^2). The important features of the model are that the vertical motions are assumed to be so small that the

coupling with the other degrees of freedom can be neglected, and the dynamical system therefore is reduced to a system of 14 first order differential equations that describe the horizontal motion of the bogie elements. All bodies are rigid, the wheel/rail kinematics and the spring and damper constitutive relations are linearized, so the only nonlinearities in the system are the contact forces between the wheels and the rails. There is a $u|u|$ term in the wheel/rail creepage/creep force relation, where u denotes the creepage. It means that the second derivative of the relation does not exist in $u = 0$. The action of the wheel flange is modeled by a very stiff linear restoring spring with a dead band δ. With q denoting the lateral displacement of a wheel set, this leads to a non-smoothness at $q = \pm\delta$, where a jump in the first derivative occurs.

The trivial solution satisfies the system for all values of the speed V, but it loses stability in a subcritical bifurcation at the speed V_H. The $u|u|$ term in the creepage/creep force relation changes the initial growth of the bifurcating periodic branch from a square root to a linear function (see True [33]), and the restoring spring creates a tangent bifurcation that stabilizes the oscillation at the lower speed the so-called critical speed V_C. At higher speeds of the bogie chaos develops (see Kaas-Petersen [17], Jensen [16] and Isaksen and True [14]).

The problem is solved numerically. Kaas-Petersen's continuation routine PATH [18] is used to calculate the bifurcation diagram for the dynamical system. PATH also calculates the eigenvalues of the Jacobian and estimates the Floquet multipliers of the Poincaré map in order to determine the stability of the various branches. Its most important feature is that it uses a mixture of time integration and Newton iteration to find the periodic solutions, whereby the computational work is reduced. A periodic solution is treated as the identity under a Poincaré map. In this way the program determines the stable and unstable solutions with the same accuracy. The Poincaré section is chosen by PATH in such a way that it is 'sufficiently transversal' to the phase space trajectory. For the numerical integrations the LSODA routine is used, which automatically switches between stiff and non-stiff solution methods whenever needed (see Petzold [26]). PATH determines the solutions with a relative error of 10^{-9}.

In the points $q = \pm\delta$ the Jacobian is not defined, and two possible ways to handle the non-smoothness were tried. First the singularity was smoothed by a hyperbolic cosine function around $q = \pm\delta$ and second the singularity was neglected and the integration simply continued across the singularity. Since no difference in the resulting dynamics could be detected, and the computation time was almost the same, the second way was chosen in the numerical investigation.

Knudsen et al. [22] and Slivsgaard and True [30] investigated the dynamics of a single-axle bogie, which is essentially only one half of the Cooperrider bogie. Knudsen proved the existence of chaos produced by the singularity in $q = \pm\delta$. For the numerical integrations Knudsen used as well the LSODA routine as an eight-stage explicit Runge–Kutta pair of order five and six. It uses variable time step and error control. To approximate the solution between the integration steps an interpolant with an asymptotic error of the same order as the global error for the numerical integration was used. The method was developed by Enright et al. [5]. This solver was chosen because it should be particularly well suited for the shadowing of a chaotic attractor. Knudsen observed that the flange forces changed continuously across the singularity in $q = \pm\delta$ and therefore the singularity was ignored in both integration methods.

Slivsgaard and True [30] also used PATH and found that the bifurcation of the periodic solution from the trivial solution is supercritical, and that the initial growth of the periodic attractor with the speed is linear. When $|q| = \delta$ a grazing bifurcation takes place and the motion becomes chaotic. It is interesting to compare the result with the bifurcations in the Cooperrider bogie model [4]. In the Cooperrider model a tangent bifurcation stabilizes the unstable periodic branch when $|q|$ grows through δ, but in Slivsgaard's single-axle bogie model the stable periodic motion becomes chaotic in a grazing bifurcation.

All the dynamical systems described above did not include the constraint of the rigid axle.

The investigation of a complete wagon model has recently been performed by Bigoni in [2]. The model employed two Cooperrider bogies attached to a car body and four wheel sets with profile S1002. Fig. 2 shows the design of the model and the location of the suspension elements. The original Cooperrider bogie uses torsional springs and dampers in the secondary suspension. They have been substituted by yaw springs and dampers. The suspension elements can be linear or non-linear.

The rail profile UIC60 with cant 1/40 combined with the wheel profile S1002 cause the appearance of multiple contact points for certain displacements of the wheel sets. These are approximated by a single patch using the method proposed by Sauvage and Pascal [28]. The static parameters for the computation of the contact forces have been obtained using the RSGEO [20] routine. The normal load can be found using the Hertz's contact theory [10] and adjusting the value with the additional penetration due to the dynamics using Kalker's work [19]. The creep forces were found using the Shen, Hedrick and Elkins non-linear theory [29].

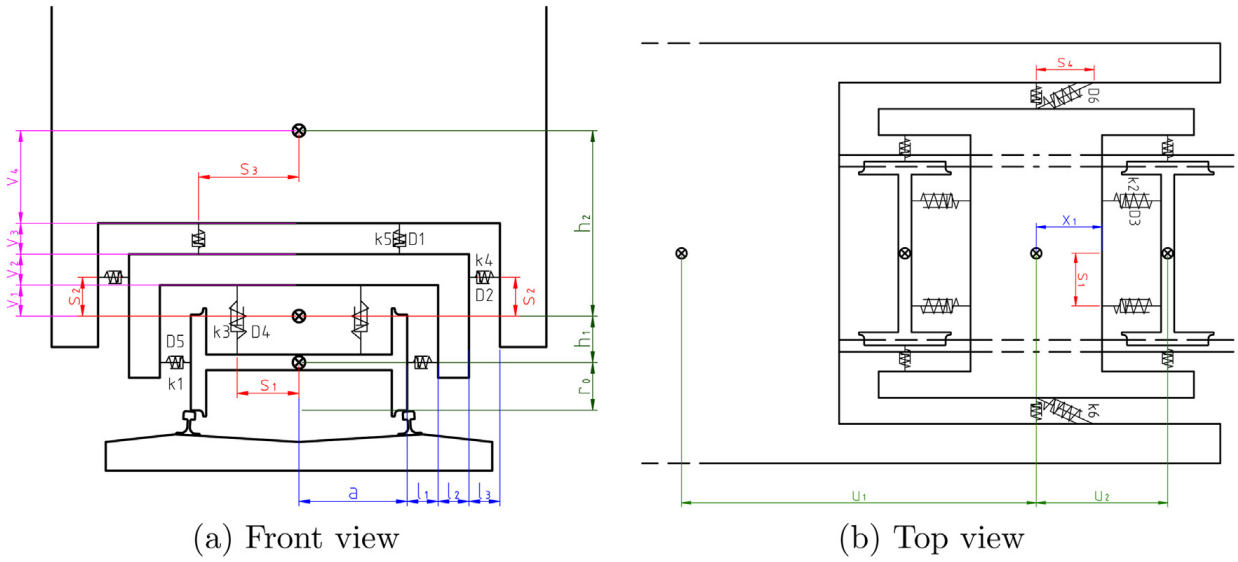

Fig. 2. Design of the Cooperrider bogie attached to a car body.

Using the formulation of the multibody problem introduced in Section 2, a system of 66 coupled first-order differential equations has been obtained. The system can be simplified using superposition when only suspension elements with linear characteristic function are used. Also the computation of the Jacobian can be sped up using the analytical values for the parts that have linear functions and using difference approximation for the wheel sets, where the contact forces are the only non-linear part of the system. These simplifications cannot be performed if the model employs non-linear suspension elements.

The dynamical problem was solved numerically using the Explicit Singly Diagonal Implicit Runge–Kutta (ESDIRK) method with appropriate initial conditions for increasing values of the speed. The ESDIRK method by Nielsen–Thomsen (ESDIRK34 NT1) [24] is a Runge–Kutta method of order 3 for the solution of stiff systems of ODE's and index one DAE's. The type of method is a 4-stage generalized linear method that is reformulated in a special semi-implicit Runge–Kutta method. The error estimation is by imbedding a method of order 4 based on the same stages as the method and the coefficients are selected for ease of the implementation. The method has 4 stages and the stage order is 2. For purposes of generating a dense output and for initializing the iteration in the internal stages a continuous extension is derived. The method is *A*-stable.

4. Models with dry friction contact

In mechanical systems with dry friction contact, with stick/slip between some bodies in the system, the degrees of freedom of the system will vary with the changes of the acting dry friction force vector. Such a system is often referred to as a structure varying system or a structural variant system. In these systems the switching boundaries that were mentioned in Section 2 must be introduced in the state space in order to define the location of the non-smoothnesses. At the switching boundaries the switch conditions must be formulated in order to define the initial conditions for the continuation of the integration of the dynamical system in the appropriate domain of the state space. In this section only one-dimensional dry friction forces occur.

Our first dynamical model of a railway vehicle with dry friction dampers with stick/slip was set up to investigate the interaction between the nonlinear dry friction damping and the nonlinear wheel/rail creep forces. Therefore the model should be so simple that the dynamical features easily can be related to this interaction without interference from other sources. True and Asmund [35] therefore started the analysis with a model of a modification of half the Cooperrider bogie. Fig. 3 illustrates the model. The stiff spring model of the action of the wheel flange in the original Cooperrider bogie was left out, and the linear wheel/rail kinematic relation and the linear characteristic of the spring was kept in place. This of course might result in unrealistically large amplitudes of the lateral motion of the wheel set.

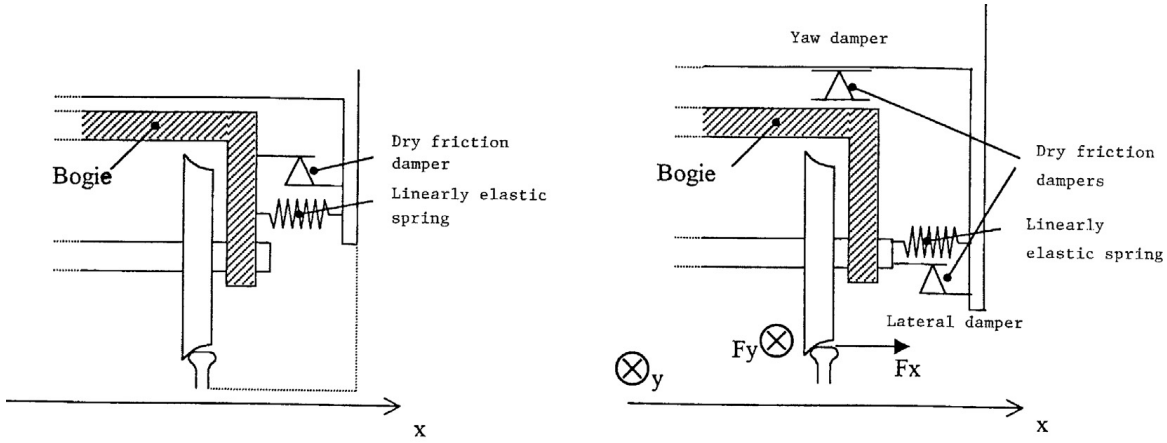

Fig. 3. The single-axle bogie with lateral dry friction damper (left) and with lateral and yaw dry friction damper (right).

The modeling of the stick/slip action in the dry friction is crucial. In order to control the jump from stick to slip in the friction relation a new heuristic smooth transition was developed and tried on some simple test cases. The results were satisfactory, and the dry friction model was therefore adopted for the vehicle model.

First the bifurcation diagram of the model with linear dampers was calculated. The dampers were laid out in such a way that the dissipation in one period of the oscillation would be approximately the same as the dissipation of the dry friction damper. Then the bifurcation diagram for the same model but now with a lateral dry friction damper and no yaw damper was calculated. The two bifurcation diagrams were plotted for comparison in Fig. 4. It is interesting to note that with the dry friction damper the bifurcation disappears and a periodic oscillation with a low amplitude exists down to very low speeds. The amplitude of the oscillation increases fast with the speed near and on the other side of the bifurcation point. Such a behavior is known from stochastic dynamical systems, and probably reflects the erratic nature of the stick/slip mechanism in the dry friction damper. We also found that the amplitude of the oscillation at speeds below the bifurcation point depends on the initial condition of the dynamical problem. At speeds below the bifurcation point there exists an entire set of equilibrium solutions to the dynamical problem but in Fig. 4 only one amplitude of one representative periodic motion out of the entire set is shown.

The dynamical system was solved numerically at discrete values of a growing speed with appropriate initial conditions. An explicit Runge–Kutta 5/6th order solver with variable step length and error control was used for the integrations of the system.

The assumption of no wheel flanges or other motion limiters is of course unrealistic. True and Trepacz [36] therefore introduced a realistic wheel/rail kinematic relation in the model and repeated the investigations. The kinematic contact

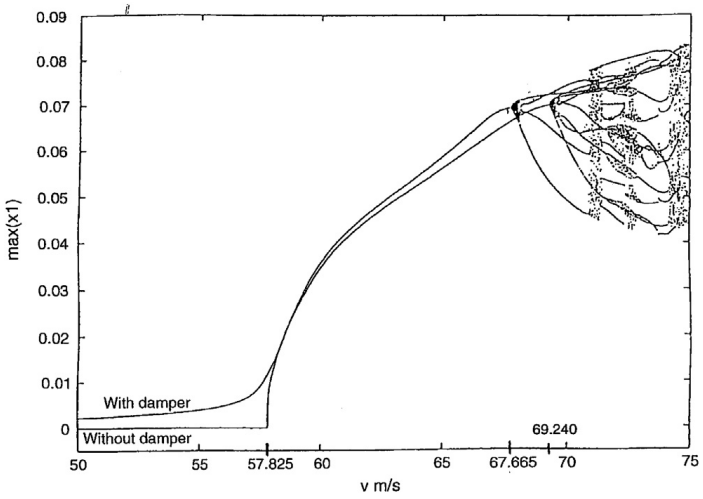

Fig. 4. Bifurcation diagrams for the single-axle bogie with and without lateral dry friction damper.

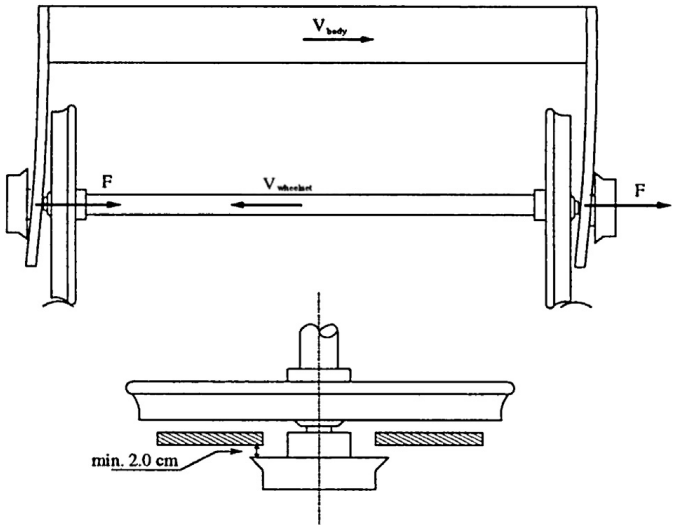

Fig. 5. The axle-guidance.

problem was solved by use of ARGE CARE's RSGEO routine [20], but again only the resultant tangent forces were taken into account in the model. In order to simplify the dynamics the horizontal component of the normal forces in the contact surface was kept constant, which of course is an unrealistic assumption.

In a real 2-axle freight wagon the motion of the axle box relative to the car body will be limited by a plate (see Fig. 5). In the lateral direction the plate acts as a linear spring with a spring constant of 1500 kN/m and a dead band of 20 mm. In the longitudinal direction the plate acts as an elastic impact with $E = 2.1 \times 10^{11}$ N/m and a dead band of 22.5 mm. E is Young's modulus for steel. This very stiff restoring force makes the dynamical system so stiff that the computation time becomes unacceptably high. We therefore approximated the impact by an ideally elastic one, where the yaw speed of the wheel set is the same before and after the impact, but its direction is reversed. We have compared some computations with either assumption and found that the dynamics remain the same, but the computation time of course increases strongly, when the impact is computed with E. If we were interested in finding the impact forces, then it would have been necessary to use the detailed model of the impact.

The limiting plate has almost no influence on the lateral dynamics, but it keeps the wheel set from derailment by limiting the maximum yaw motion. The motion is chaotic, see Fig. 6, where the maximum amplitudes of the lateral oscillations of the wheel set are plotted versus the speed of the vehicle.

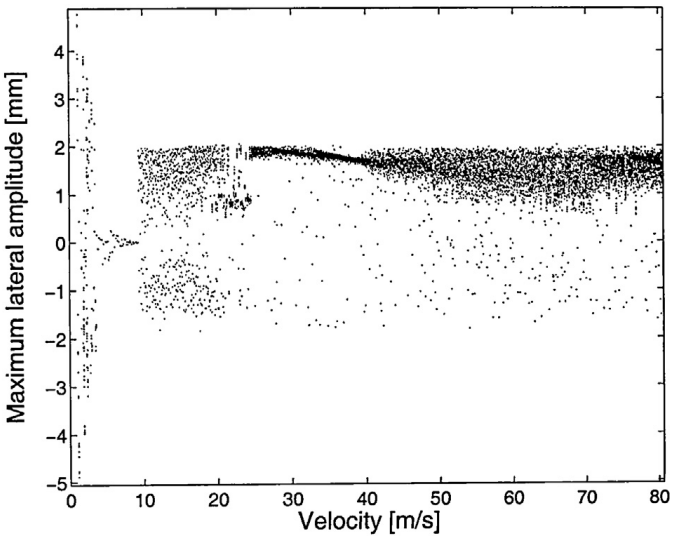

Fig. 6. Illustration of the chaotic motion of the attractor.

Fig. 7. A 4-axle Chinese hopper wagon.

The dynamical system was solved numerically, initially with MATLAB's routine `ode45`, but then using an explicit Runge–Kutta/Cash/Karp 5/6th order solver with adaptive step size and error control. The speed of the computations with the Runge–Kutta method was around 1000 times faster than when MATLAB was used. MATLAB was, however, used for the post-processing. The time of the impact, when the yaw speed changes direction, was approximated by the time in the time stepping sequence when the axle box had penetrated the guiding plate. In the case of linear elastic impact the instants, when the axle box hit the plate and when it left the plate again, were calculated more accurately by a Newton iteration. In the time interval of the impact the forces on the axle box were supplemented by the elastic reaction forces of the plate.

5. Realistic railway vehicle models

5.1. The 4-axle hopper wagon on three-piece freight trucks

Xia and True [38,39] investigated the dynamics of a 4-axle empty Chinese hopper wagon on a straight track. The wagon (see Fig. 7) runs on two 'three-piece freight trucks' (bogies) (see Fig. 8) that are the most used bogies worldwide

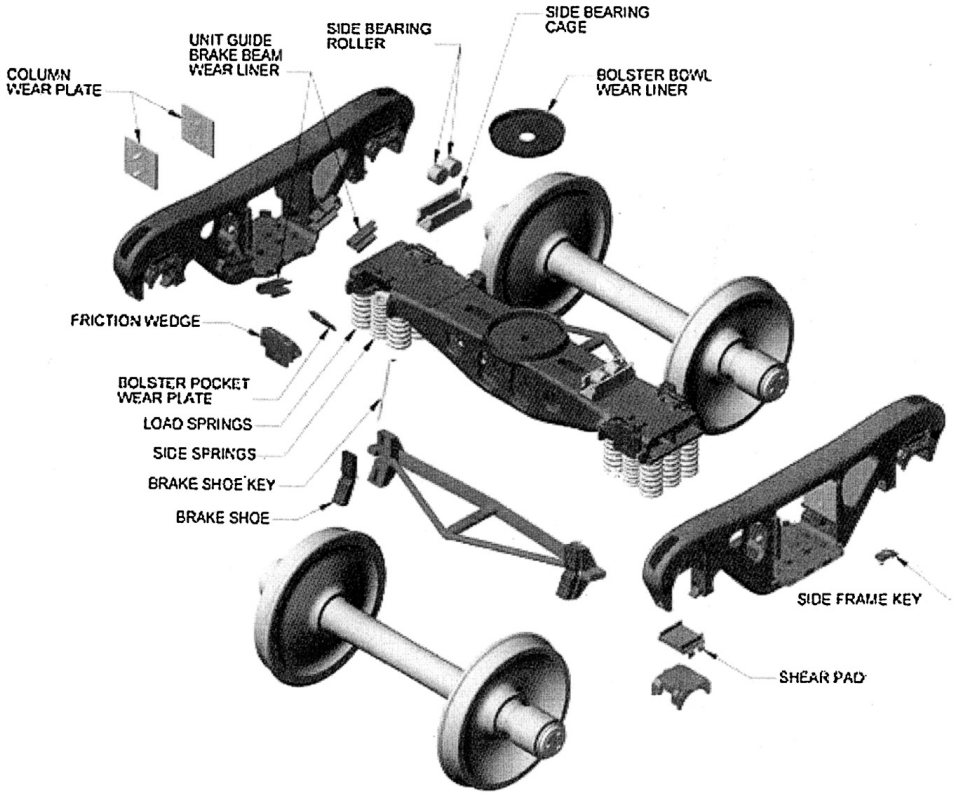

Fig. 8. Three-piece freight truck (bogie).

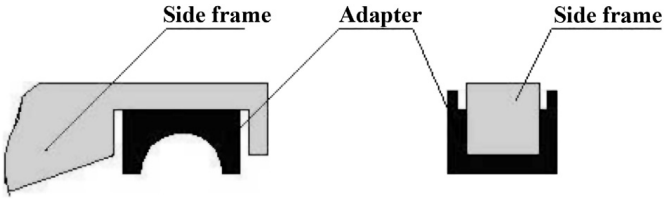

Fig. 9. The contact between the end of a frame and an adapter.

due to their simplicity, robustness and low price. The dynamics, however, leaves something to be desired. The dynamical model has 81 degrees of freedom (DOF) and is loaded with 'non-smoothnesses'. First there are the non-smoothnesses in the wheel/rail kinematic relations that we have seen earlier in this work. In addition – and that is unique for this design – all the damping is performed by dry friction with stick/slip between plane surfaces under a dynamically varying normal load. The axle boxes are fit with adapters that carry the bogie frames. The adapters can slide longitudinally under the bogie frames with dry friction contact between stops that limit their relative horizontal motion (see Fig. 9). In the only (the secondary) suspension system between the bolster and the car body (see Fig. 10) the vertical as well as the lateral damping of the relative motion are performed by dry friction with stick/slip between spring loaded wedge shaped blocks that are called 'snubbers'. Since the occurrence of stick or slip between the snubbers depends both on the normal pressure and the resulting shear force between the contacting surfaces the contact forces establish a non-smooth coupling between the horizontal and vertical components of the forces and thereby also between the horizontal and vertical dynamics. Under the influence of the dynamic forces the blocks may separate from the bolster or from the side frame, which is the source of another non-smoothness in the dynamical system. The rolling between the car body and the bogie frames is limited by bumper stops that are modelled as very stiff vertical springs with a dead band. The friction forces on the surfaces of the bumper stops are integrated into the non-smooth yaw friction torque on the car body and bolsters. Xia used the smoothened heuristic dry friction model that was used in the works in [35, Section 4]. He extended the application to two-dimensional dry friction forces on a plane. Xia introduced a friction direction angle, which replaces the sign function used in the one-dimensional dry friction analysis. The wheel/rail kinematics was calculated by his own routine WRKIN. For a description of the total model and the detailed formulation of the dynamical system the interested reader is referred to Xia's thesis [37].

Xia's main results were described in the two bifurcation diagrams in Fig. 11. The left diagram was made for growing speed and the right one for decreasing speed. The hysteresis is clearly visible. Below $V = 16$ m/s the equilibrium solutions found may be a set valued stationary motion or a combination of set valued stationary and periodic motions. A typical result for such a motion is shown in Fig. 12. At the supercritical bifurcation from the 'zero' solution on the left diagram a stable periodic solution develops. It only exists in a short speed interval after which it changes into a chaotic motion. For decreasing speed the chaotic attractor is found all the way down to 21 m/s, where it disappears – probably in a crisis. The maximum speed of the car in normal use is below 30 m/s–108 km/h. In Fig. 13 we show the chaotic lateral displacements of the four wheel sets at $V = 29$ m/s. As far as it is possible the results have been compared with tests of the dynamics of a real hopper car on a railway line, and the test results agree well with the theoretical values.

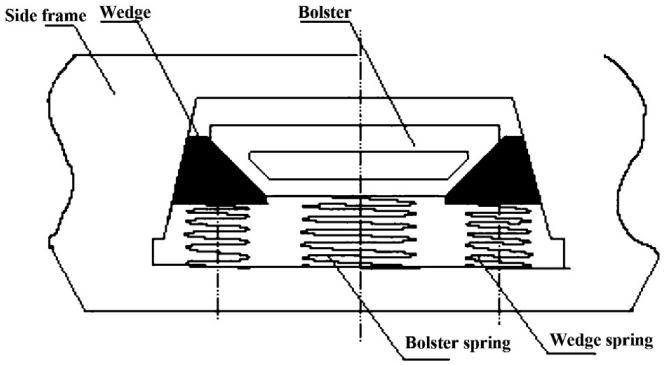

Fig. 10. A cross-section of the wedge dampers in the three-piece freight truck.

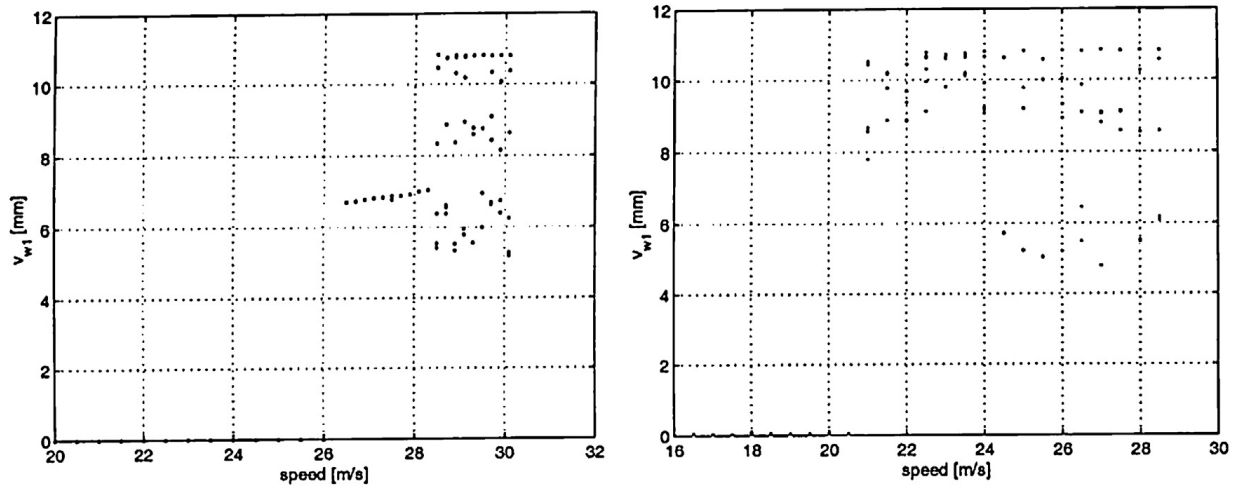

Fig. 11. Bifurcation diagrams for the Chinese hopper wagon. Left for increasing speed, right for decreasing speed.

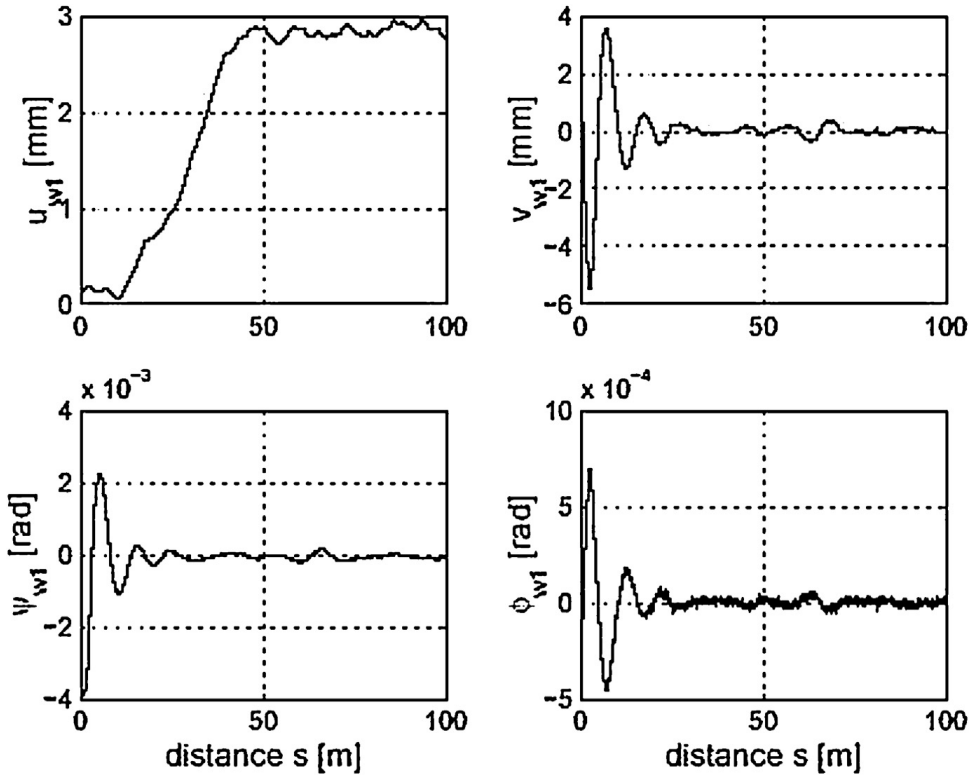

Fig. 12. The motions of the leading wheel set of the leading bogie at speed $V = 20$ m/s. Top left: the longitudinal displacement, top right: the lateral displacement, bottom left: the yaw angle and bottom right: the roll angle.

Xia used MATLAB for his calculations. The calculations were therefore very time consuming. The bifurcation diagram in Fig. 11 needed one week of shared computer time on the cluster of the DTU Informatics department(!)

The entire dynamical system with its constraint equations is a differential-algebraic system with index-3. The system was, however, transformed into an index-1 system by a differentiation with respect to time of the algebraic stick-constraint equations in the system. The index-1 system was then integrated in the domains where the state variables changed continuously by the Runge–Kutta solver `ode45` from MATLAB because it is effective. The system is stiff, and first the `ode45` solver was used, and if it failed then an implicit method was used. Due to the discontinuities each step of the integration of the system proceeded in eight steps with a loop. The details can be seen in Xia [37], where also the detailed derivation of the switch conditions are found.

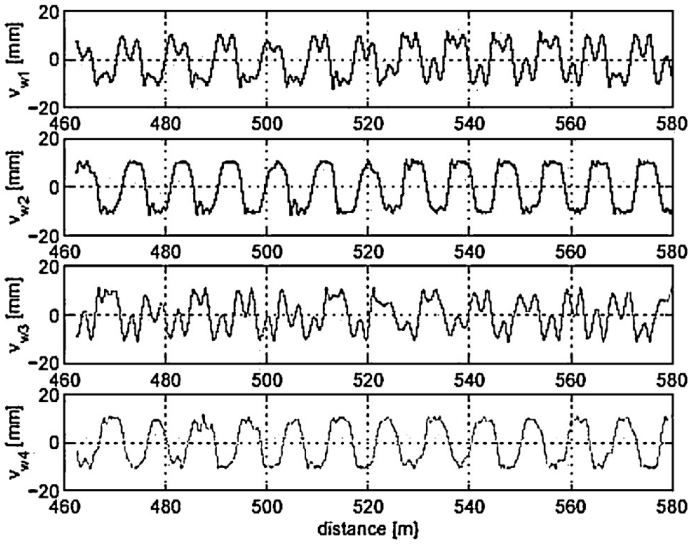

Fig. 13. The lateral displacements of the wheel sets at the speed $V = 29$ m/s as a function of the distance after the transients are negligible. From top to bottom: The leading wheel set in the leading bogie, the trailing wheel set in the leading bogie, the leading wheel set in the trailing bogie and the trailing wheel set in the trailing bogie.

Fig. 14. The Hbbills 311 wagon.

5.2. *The 2-axle freight wagon with a standard UIC-suspension*

Mark Hoffmann investigated the dynamics of two-axle European freight wagons with the UIC standard suspension [11–13]. One wagon is shown in Fig. 14, and its long wheelbase of 10 m distinguishes the wagon from the majority of two-axle wagons. The construction data were given to us from The German Railways, DB AG, in Minden. The UIC suspension (see Fig. 15) consists of two double links that connect the car body with a leaf spring that rests on an axle box. The links act as a pendulum suspension in both the lateral and longitudinal direction with combined rolling and sliding friction with stick/slip in the bearings. When the lateral displacement of a link becomes large, then the lower link will hit the bracket and the pendulum length will be halved for the further motion. The leaf spring damps the vertical motions through dry friction sliding with stick/slip between the steel leafs of the spring, and it also acts with a restoring force on the vertical motion through bending of the leafs. The mathematical model of the leaf springs that are used on the wagons was formulated by Fancher et al. [6]. The dissipated work is measured by the areas of the hysteresis loops created in the dry friction surfaces by the dynamics. Piotrowski [27] formulated the mechanical and mathematical models for the action of the links (see Fig. 16) on the basis of measurements of the behavior of a real suspension in his laboratory. They are shown in Fig. 17a and b. Piotrowski also gave values for the parameters in his models. Hoffmann has demonstrated how accurately the measured hysteresis loop in the laboratory can be approximated by Piotrowski's model when the model parameters are chosen appropriately (see Fig. 18). The wheel sets are restrained by a guidance plate with a dead band of 22.5 mm in the longitudinal and 20 mm in the lateral direction. The action of the guidances is explained in Section 4 by True and Trzepacz. Hoffmann handles the non-smoothnesses in the dynamic problem

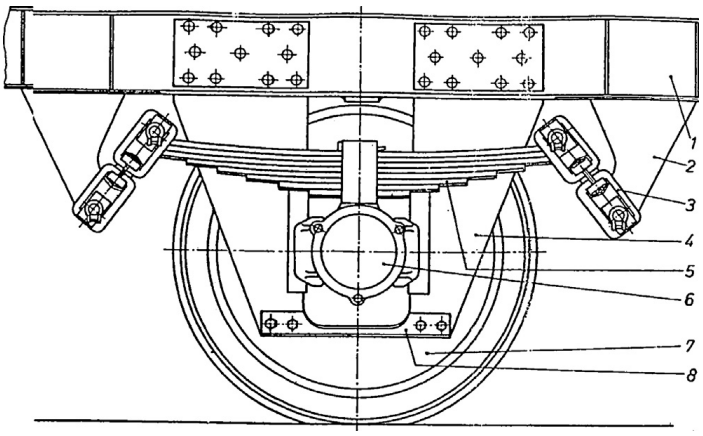

Fig. 15. The UIC standard suspension.
Reproduced from the book 'Laufwerke', Transpress, 1986.

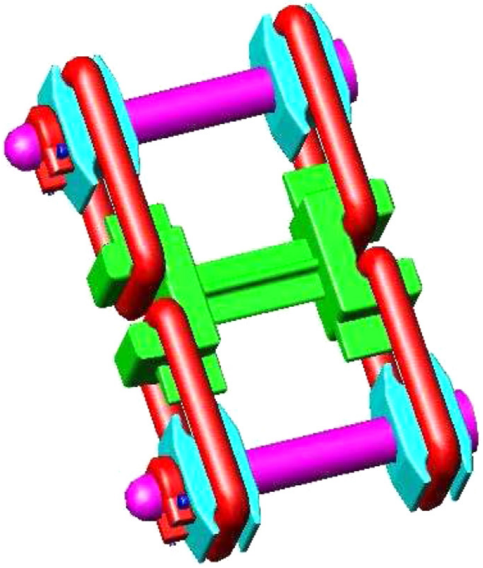

Fig. 16. The links of the UIC standard suspension.

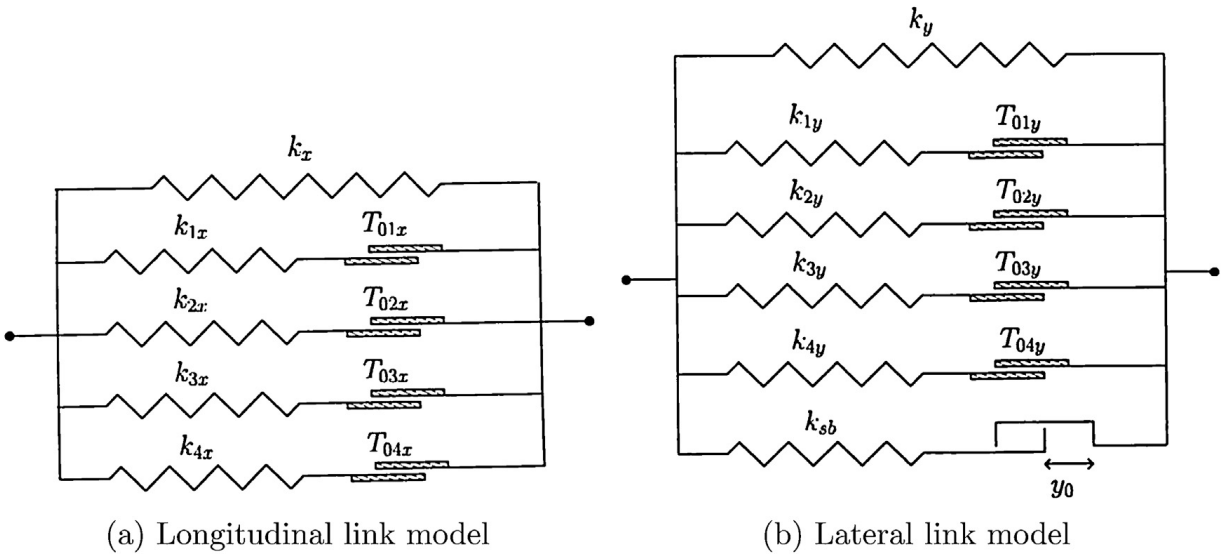

(a) Longitudinal link model (b) Lateral link model

Fig. 17. The link models.

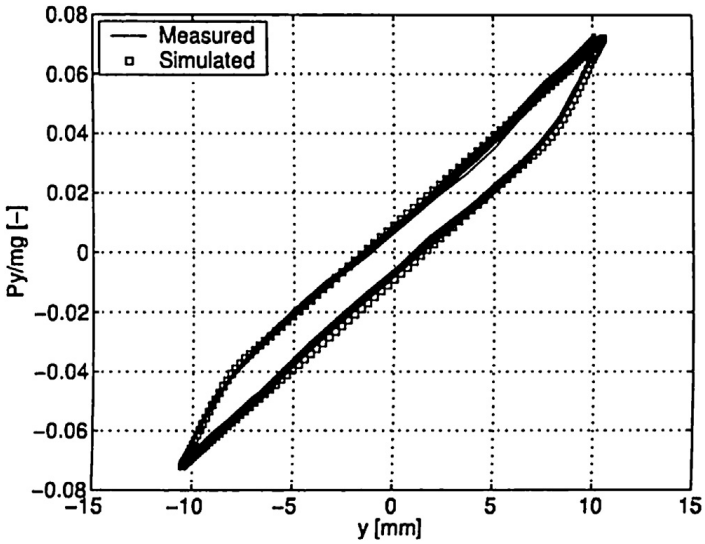

Fig. 18. A comparison between the mathematical model and the measured hysteresis loop.

through a definition of the switching boundaries and event detection. In Hoffmann's model the car body and the axles all have their own degrees of freedom, and the calculation of the instances of events when a trajectory hits a switching boundary therefore becomes much more elaborate than was the case in our earlier examples.

The non-smoothness is due to the nature of the interacting forces, i.e., stick–slip transitions in the suspension model, impacts between the axle box and axle guidance and discontinuities in the contact parameters for the wheel–rail contact. Classical solvers are all based on the existence of the derivatives of the function $\mathbf{F}$ (see Section 2). The non-smoothnesses tend to have the following effect on the numerical method: (1) the numerical solution is simply inaccurate because the progress of the solution is based on non-existing derivatives of $\mathbf{F}$. This is a common situation for constant step size integration schemes. (2) The simulation time is unacceptably high because the step size is forced down near the non-smooth points in order to satisfy the specified error tolerance. This happens when integration schemes with variable step size and error control are applied, but it is due to the lack of smoothness of the local error. The interested reader is referred to Hoffmann's thesis [11] for a deeper discussion of the solution of this problem.

Hoffmann illustrated the importance of the location of the events. He investigated a model hysteresis loop and plotted the discrete solution points that were calculated by the ESDIRK34 NT1 solver with step and error control and event location and compared the result with the discrete solution points that were calculated with the same solver but without event location (see Fig. 19). The comparison between the figures clearly demonstrates the increase in the

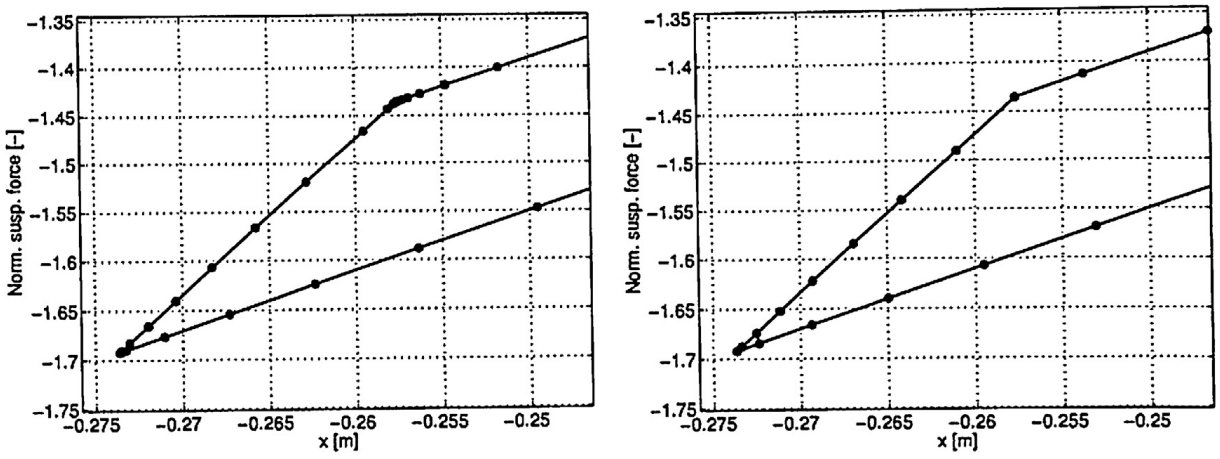

(a) Without event location (b) With event location

Fig. 19. The time steps on the hysteresis loop.

number of steps without the event location, which results in a larger computational effort. It should be noted that the number of distinguishable points in the left hand corner in Fig. 19a, may be misleading, because several points may be lying so densely that the eye cannot separate them.

It is also evident from Fig. 19a that the computation time would increase enormously if a solver with constant step size had been applied. Such a solver will namely need a step size that is determined by the density of the points in the corners in order to satisfy the given error tolerance. Since the step size is constant the solver must use the same step size also in the integration along the linear sections.

Hoffmann compared the dynamics of the different types of freight wagons with UIC standard suspension. His results were presented on time series plots and bifurcation diagrams. The dynamics is very complicated with set valued stationary as well as periodic, multi-periodic and chaotic motions. He found subcritical and supercritical bifurcations into the various kinds of behavior caused by shear force instabilities and nonlinear resonances as well as symmetry breaking bifurcations. The interested reader is referred to Refs. [11–13].

The dynamical system is integrated with ESDIRK34 NT1 already mentioned in –Section 3.

The solution to the initial value problem is found by a piecewise integration strategy where each smooth section is integrated separately. The isolated events are located during the integration and treated independently. It is crucial to locate the non-smooth events during the integration. The events are determined by root finding of the event functions that define the switching boundaries between the different states of the model. For the details of the procedure the interested reader is referred to Hoffmann [11, Section 3.2].

Newton–Raphson's method needs the Jacobi matrix of the dynamical system. In our case it is a sparse matrix with $68 \times 68 = 4624$ elements of which very many are zero. Therefore the dependencies of the function $\mathbf{F}$ are identified before the integration starts, and only the non-zero elements are computed. The entries in the Jacobi matrix are computed in a column-wise fashion because the relative kinematics and interacting forces that are computed for the relative perturbations related to x_j can be reused for all non-zero elements in the jth column.

6. Discussion of numerical methods and challenges

The formulation of railway vehicle dynamical systems based on the physical principles (3) and (4) can be expressed in the form of a general initial value problem (1). In general there will be no closed form solution except the trivial state solution obtained at low speed and the models are typically both nonlinear and are subject to non-smoothness (for example in wheel–rail contact and suspension forcing). From a practitioners viewpoint, to solve such systems numerically demands the use of suitable numerical methods for the control of robustness, accuracy and efficiency. These properties are essential and without them it can be difficult to establish improved insight into the critical model behavior. A general class of numerical methods for solving (1) that have good support for local error estimation (for use with step size controllers) and event detection for non-smooth problems is the one-step/multi-stage Runge–Kutta methods.

The general class of m-stage Runge–Kutta (RK) methods for advancing (1) a single time step $\Delta t_n = t_{n+1} - t_n$ is given as

$$\begin{aligned} \mathbf{g}_i &= \mathbf{x}^n + \Delta t_n \sum_{j=1}^{m} a_{ij} \mathbf{F}(\mathrm{g_j}, t_n + c_j \Delta t_n; \mathbf{P}) \\ \mathbf{x}^{n+1} &= \mathbf{x}^n + \Delta t_n \sum_{j=1}^{m} b_j \mathbf{F}(\mathrm{g_j}, t_n + c_j \Delta t_n; \mathbf{P}) \end{aligned} \tag{16}$$

The coefficients of a convergent numerical scheme are typically given in terms of a Butcher Tableau [3] defined in terms of $\mathbf{A} \in \mathbb{R}^{m \times m}$, $\mathbf{b} \in \mathbb{R}^m$ and $\mathbf{c} \in \mathbb{R}^m$. A Runge–Kutta method is said to be order p if the local truncation error behaves asymptotically as $\mathcal{O}(\Delta t^p)$ for fixed step sizes [23]. For computations one should only use methods which have order $p > 1$ in practice due to accuracy concerns. This rules out Euler's explicit method. Local errors committed during one time step using (16) will be $\mathcal{O}(\Delta t^{p+1})$. Such errors can be estimated by comparing the computed approximate

solution $\mathbf{x}^{n+1}$ to one computed using an embedded Runge–Kutta method. This local error estimate can for efficiency reasons be based on the same intermediate Runge–Kutta stage values using the following formula

$$E^{(m)} = \Delta t_n \sum_{j=1}^{m} d_j \mathbf{F}(\mathrm{g_j}, t_n + c_j \Delta t_n; \mathbf{P}) \tag{17}$$

where $\mathbf{d} \in \mathbb{R}^m$. If the local error estimate is used for variable step size control, it is often possible to significantly improve efficiency over fixed step size time integration by using a variable step size controller that tries to maintain a constant accuracy level. The use of step size control has the added advantage that at the same time robustness is improved because thereby exponential growth of errors that may develop due to choices of step size will not be permitted.

The local error should be compared to user-defined acceptable error tolerances, respectively, absolute ϵ_a and relative ϵ_r levels of accuracy. In case of non-smoothness such local error estimates may become unreliable because local smoothness and asymptotic behavior of the solution is assumed. For this reason, several time steps may be rejected before the time step sizes have been reduced sufficiently for the error to be acceptable, in which case effort is wasted but the accuracy is maintained.

Dynamical systems for railway vehicles can exhibit significant stiffness due to the presence of widely different dynamical time scales in the models. For stiff systems, stability and not accuracy imposes a constraint on valid choices of the step sizes and may require significant reductions in the step sizes for securing stability. Explicit numerical schemes have bounded stability regions and therefore they may incur a performance penalty in such cases – in particular when the step size is governed by stability needs rather than accuracy. For this reason, it is customary to choose implicit solvers, which formally have large absolute (linear) stability regions. In practice, implicit Runge–Kutta methods require for each time step finding a sufficiently accurate root of the nonlinear system $\mathbf{G}(\mathbf{z}) = \mathbf{0}$ for the vector of unknown $\mathbf{z} = \left(\mathbf{g}_1^{n+1}, \ldots, \mathbf{g}_m^{n+1}\right) \in \mathbb{R}^{2Nm}$. For stiff problems this is typically done using Newton–Raphson's iterative method, which can be expressed as a two-recurrence in the compact form

$$\mathbf{z}^{k+1} = \mathbf{z}^k + \boldsymbol{\delta}^k, \quad \boldsymbol{\delta}^k = -\mathbf{J}^{-1}\mathbf{r}^k, \quad k = 0, 1, \ldots. \tag{18}$$

where $\mathbf{J} = \partial \mathbf{G}(\mathbf{z})/\partial \mathbf{z}|_{\mathbf{z}=\mathbf{z}^k}$ is a Jacobian matrix of the system and $\mathbf{r}^k = \mathbf{G}(\mathbf{z}^k)$ is the residual of the nonlinear system in the kth iteration. For non-smooth problems, the Jacobian matrix can be singular or ill-conditioned in a point and this can be the cause of numerical problems if event detection is not used [11]. Reduction in solution effort per time step of the Runge–Kutta method is typically achieved by exploiting properties in the coefficients of $\mathbf{A}$ and/or using an inexact constant approximation to $\mathbf{J}$ in the inner solve step for determining $\boldsymbol{\delta}^k \approx \mathbf{z}^k - \mathbf{z}$. However, this may be at the expense of slowed down convergence rates and a resulting decrease in algorithmic efficiency which needs to be balanced by improved numerical efficiency. A class of Runge–Kutta schemes that is subject to the idea of minimizing the work effort per step and also have good stability properties are the ESDIRK methods. A suitable stopping criterion for the Newton–Raphson method is based on making sure that a measure of the estimated errors $\boldsymbol{\delta}^k$ in the inner loop of each Runge–Kutta stage is sufficiently small for the errors committed in one complete Runge–Kutta step to be dominant.

A number of pre-packaged scientific solvers for the solution of systems of ordinary differential equations exist (e.g., see http://www.netlib.org) but details will not be given. However, they will be referenced in the following where appropriate.

Performance is another key concern for practical use of solvers. It can be useful to evaluate the performance of a numerical scheme in terms of algorithmic and numerical efficiencies. The algorithmic efficiency is measured in terms of iteration counts (successful/failed steps and function evaluations), and the numerical efficiency is a direct measure of wall clock time. To compare alternative methods the step size history needs to be taken into account and a fair comparison can be done by using the same step size control for each method together with a specification of the same acceptable tolerance level. As an example, a recent investigation of the dynamics of the Cooperrider's bogie model shown in Fig. 2 has been performed on a straight track at $V = 40$ m/s (not hunting) and $V = 120$ m/s (hunting) using two different RK methods with same step size control and different tolerance levels. In Fig. 20 we present computed results obtained with the package SDIRK [25] which includes a PI step size control strategy (e.g., see [8]). The basic version of the package contains the ESDIRK34 NT1 method by Nielsen–Thomsen [24] and the code has been extended to include an Explicit Runge–Kutta–Fehlberg method ERKF34 [9], for use in combination with the existing PI controller to make comparisons fair. A detailed breakdown of important performance characteristics is given in Table 1. It is

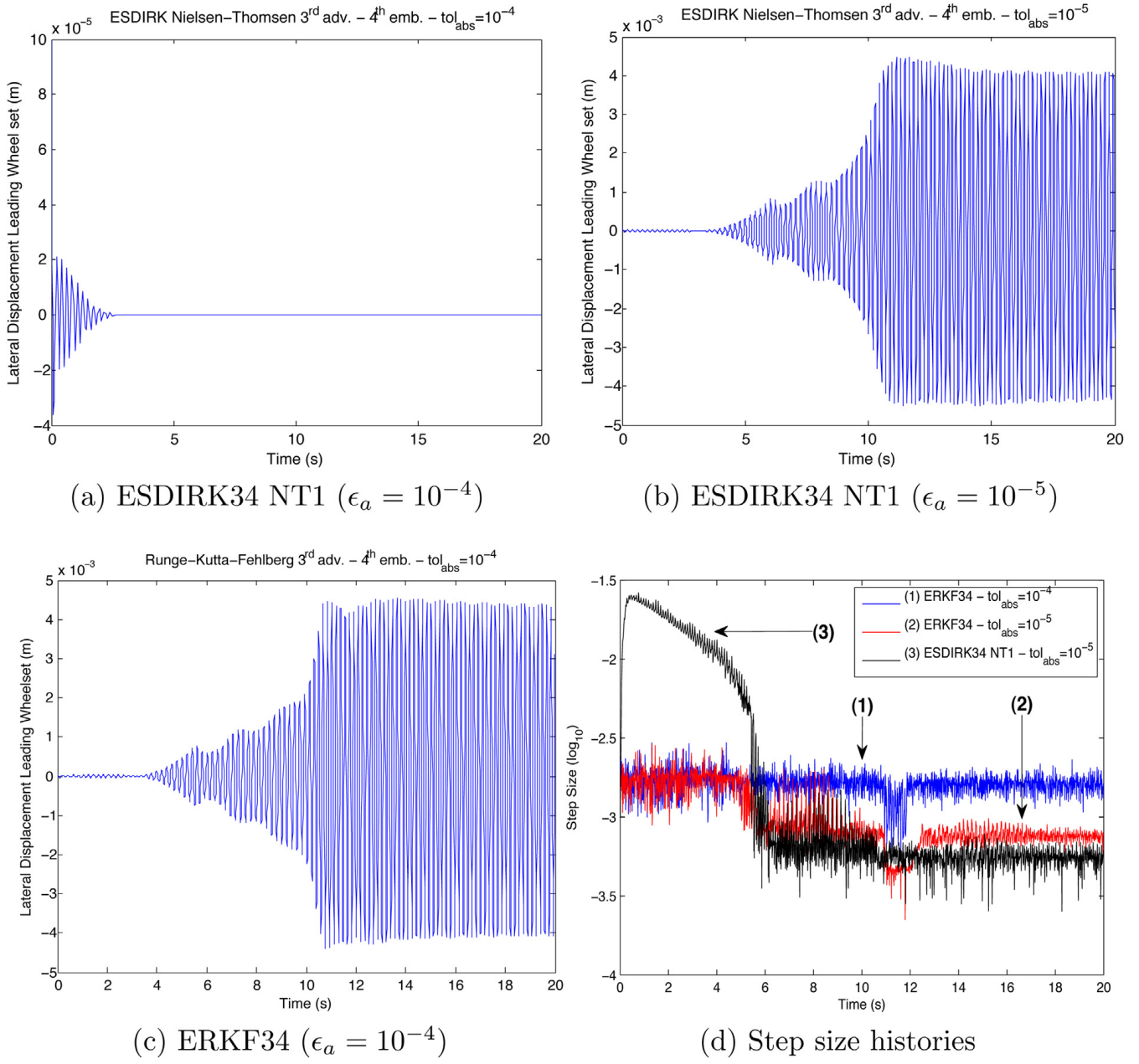

Fig. 20. Computed results for lateral displacement of leading wheel set of Cooperrider's bogie model for different user-defined absolute tolerance levels. Using ESDIRK34 NT1 it is found that (a) the transient behavior is fully damped for $\epsilon_a = 10^{-4}$ and (b) periodic oscillations (hunting) are captured for $\epsilon_a = 10^{-5}$. With ERKF34 it is found that (c) periodic oscillations (hunting) are captured already at $\epsilon_a = 10^{-4}$.

Table 1
Performances of the RKF34 and ESDIRK34 NT1 for solving a transient analysis of 20 s of a Cooperrider model hunting. The table shows the absolute tolerance used, the method's names, the wall clock time, the number of function evaluations, the number of Jacobian evaluations, the number of accepted steps and the number of rejected steps. ESDIRK34 NT1 with tolerance 10^{-4} fails in detecting the hunting phenomenon.

ε_a	Solver	CPU time	# Fun. ev.	# Jac. ev.	# Acc.	# Rej.
10^{-4}	ERKF34	15.34 s	74,505		12,617	6009
	ESDIRK34 NT1	1.47 s	1181	112	90	20
10^{-5}	ERKF34	21.25 s	130,389		22,989	9613
	ESDIRK34 NT1	467.12 s	428,957	34,911	25,525	9385

noticeable that the hunting phenomenon can be captured using the explicit ERKF34 but not the implicit ESDIRK34 at a tolerance level $\epsilon_a = 10^{-4}$. The reason is that the implicit method exhibits strong numerical damping of these high frequency modes at this tolerance level. With a reduced tolerance level $\epsilon_a = 10^{-5}$ the implicit ESDIRK34 has reduced numerical damping of the hunting modes and captures the phenomenon. However, it has a wall clock time which is close to 22 times larger as a result of more work per step compared to the explicit solver for this tolerance level. This result challenges the wide use of implicit methods instead of explicit methods. It also highlights the importance of tuning the (usually user-defined) tolerance level to be able to resolve a physical phenomenon of interest. It demonstrates that explicit solvers from a performance viewpoint can be more attractive for both efficient and accurate analysis than an alternative implicit method of similar formal accuracy.

7. Lessons learned

It is highly recommended to employ numerical schemes for dynamic railway vehicle simulations which employ variable step size control for control of local errors (targets efficiency, robustness and accuracy), introduce the relevant switching boundaries in the model formulations (targets accuracy and efficiency) and make use of event location for the numerical solution of non-smooth dynamical problems (targets accuracy and efficiency). Final results should be subject to convergence tests to rule out the possibility of errors, which may arise from the choice of too relaxed tolerance levels. For numerical investigation of chaotic dynamics we have experienced that explicit solvers may have an advantage over implicit solvers, because for accurate results the step size is bound by accuracy rather than stability requirements and the explicit methods require less work per step for same formal order of accuracy.

The time spent with the formulation of the root finding method for determination of the events and of the laws that apply in the events is a cheap investment in a numerical routine that then will operate much faster and yield reliable results. If however the switching boundaries lie very close together in the state space other strategies may apply, see e.g., Studer and Glocker [31], where a modified scheme is applied.

References

[1] M. Arnold, B. Burgermeister, C. Führer, G. Hippmann, G. Rill, Numerical methods in vehicle system dynamics: state of the art and current developments, Vehicle System Dynamics 49 (2011) 1159–1207.
[2] D. Bigoni, Curving Dynamics in High Speed Trains, Master's thesis, IMM, The Technical University of Denmark, Kongens Lyngby, Denmark, 2011.
[3] J. Butcher, Numerical Methods for Ordinary Differential Equations, J. Wiley, Chichester, West Sussex, England, Hoboken, NJ, 2003.
[4] N. Cooperrider, The hunting behavior of conventional railway trucks, ASME Journal of Engineering and Industry 94 (1972) 752–762.
[5] W.H. Enright, K.R. Jackson, S.P. Nørsett, P.G. Thomsen, Interpolants for Runge–Kutta formulas, ACM Transactions on Mathematical Software 12 (1986) 193–218.
[6] P.S. Fancher, R.D. Ervin, C.C. MacAdam, C.B. Winkler, Measurement and representation of the mechanical properties of truck leaf springs, SAE Transactions (1980).
[7] V.K. Garg, R.V. Dukkipati, Dynamics of Railway Vehicle Systems, Academic Press, Toronto, Orlando, San Diego, New York, London, Montreal, Sydney, Tokyo, 1984.
[8] K. Gustafsson, Control of Error and Convergence in ODE Solvers, Ph.D. thesis, Department of Automatic Control, Lund Institute of Technology, 1992.
[9] E. Hairer, S.P. Nørsett, G. Wanner, Solving Ordinary Differential Equations I: Nonstiff problems, Solving Ordinary Differential Equations I: Nonstiff Problems, Springer Series in Computational Mathematics, second revision ed., Springer-Verlag, Berlin, Wien, New York, 1991.
[10] H. Hertz, Über die Berührung fester elastischer Körper, Journal für die Reine und Angewandte Mathematik 92 (1881) 156–171.
[11] M. Hoffmann, Dynamics of European Two-axle Freight Wagons, Ph.D. thesis, IMM, The Technical University of Denmark, http://www2.imm.dtu.dk/pubdb/views/publication_details.php?id=4853, 2006.
[12] M. Hoffmann, H. True, On the dynamics of a railway freight wagon with UIC standard suspension, in: I. Zobory (Ed.), Proc. 9th Miniconf. on Vehicle System Dynamics, Identification and Anomalies, Budapest, November 8–10, 2004, Budapest University of Technology and Economics, Budapest, Hungary, 2006, pp. 91–98.
[13] M. Hoffmann, H. True, The dynamics of european two-axle railway freight wagons with UIC standard suspension, in: J.K. Hedrick (Ed.), Proc. 20th IAVSD Symposium of The International Association for Vehicle System Dynamics, Taylor & Francis, 2008, pp. 225–236.
[14] P. Isaksen, H. True, On the ultimate transition to chaos in the dynamics of cooperrider's bogie, Chaos, Solitons and Fractals 8 (1997) 559–581.
[15] S. Iwnicki (Ed.), The Manchester Benchmarks for Rail Vehicle Simulation, Vehicle System Dynamics, vol. 31, Supplement, Swets & Zeitlinger, Lisse, 1999.
[16] C.N. Jensen, H. True, On a new route to chaos in railway dynamics, Nonlinear Dynamics 13 (1997) 117–129.
[17] C. Kaas-Petersen, Chaos in a railway bogie, Acta Mechanica 61 (1986) 89–107.

[18] C. Kaas-Petersen, PATH – User's Guide, Technical Report, Department of Applied Mathematical Studies and Centre for Nonlinear Studies, University of Leeds, 1989.
[19] J. Kalker, wheel–rail rolling contact theory, Wear 144 (1991) 243–261.
[20] W. Kik, D. Moelle, ACRadSchiene – To create or Approximate Wheel/Rail profiles, Technical Report, 2010.
[21] K. Knothe, F. Böhm, History of stability of railway and road vehicles, Vehicle System Dynamics 31 (1999) 283–323.
[22] C. Knudsen, R. Feldberg, H. True, Bifurcations and chaos in a model of a rolling wheelset, Philosophical Transactions of the Royal Society A 338 (1992) 455–469.
[23] R. Leveque, Finite Difference Methods for Ordinary and Partial Differential Equations: Steady-State and Time-Dependent Problems (Classics in Applied Mathematics), SIAM, Society for Industrial and Applied Mathematics, Philadelphia, USA, 2007.
[24] H.B. Nielsen, P.G. Thomsen, Hæfte 66 – Numeriske Metoder for Sædvanlige differentialligninger, Numerisk Institut, DTH, 1993.
[25] E. Østergaard, Documentation for the SDIRK C++Solver, Technical Report 2, IMM, Technical University of Denmark, 1998.
[26] L. Petzold, Automatic selection of methods for solving stiff and nonstiff systems of ordinary differential equations, SIAM Journal on Scientific and Statistical Computing 4 (1983) 136–148.
[27] J. Piotrowski, Model of the UIC link suspension for freight wagons, Archive of Applied Mechanics 73 (2003) 517–532.
[28] G. Sauvage, J.P. Pascal, Solution of the multiple wheel and rail contact dynamic problem, Vehicle System Dynamics 19 (1990) 257–272.
[29] Z.Y. Shen, J.K. Hedrick, J.A. Elkins, A comparison of alternative creep-force models for rail vehicle dynamic analysis, in: J.K. Hedrick (Ed.), The Dynamics of Vehicles, Proc. 8th IAVSD Symp., Cambridge, MA, Swets and Zeitlinger, Lisse, 1984, pp. 591–605.
[30] E. Slivsgaard, H. True, Chaos in Railway-vehicle Dynamics, Nonlinearity and Chaos in Engineering Dynamics, John Wiley & Sons Ltd, Chichester, 1994, pp. 183–192.
[31] C. Studer, C. Glocker, Simulation of non-smooth mechanical systems with many unilateral constraints, EUROMECH Newsletter 29 (May 2006) 15–33.
[32] P.G. Thomsen, H. True (Eds.), Non-smooth Problems in Vehicle Systems Dynamics, Proc. Euromech 500 Colloquium, Springer, Berlin, Wien, New York, 2010.
[33] H. True, On a new phenomenon in bifurcations of periodic orbits, in: Dynamics, Bifurcation and Symmetry, New Trends and New Tools, September 3–9, 1993, Kluwer Academic Publishers, P.O. Box 322, NL-3300 AH Dordrecht, The Netherlands, 1994, pp. 327–331.
[34] H. True, Dynamics of railway vehicles and rail/wheel contact, Dynamics of Railway Vehicles and Rail/Wheel Contact, CISM Courses and Lectures – No. 497, Springer, Wien, New York, 2007, pp. 75–128.
[35] H. True, R. Asmund, The dynamics of a railway freight wagon wheelset with dry friction damping, Vehicle System Dynamics 38 (2002) 149–163.
[36] H. True, L. Trzepacz, The dynamics of a railway freight wagon wheelset with dry friction damping in the suspension, in: Proc. 18th IAVSD Symposium on Vehicle System Dynamics, The Dynamics of Vehicles on Roads and Tracks, Taylor & Francis, London, UK, 2004, pp. 587–596.
[37] F. Xia, The Dynamics of The Three-Piece-Freight Truck, Ph.D. thesis, IMM, The Technical University of Denmark, http://www2.imm.dtu.dk/pubdb/public/search.php?searchstr=Fujie+Xia&n=5&searchtype=strict, 2002.
[38] F. Xia, H. True, On the dynamics of the three-piece-freight truck, in: RTD, vol. 25, IEEE/ASME Joint Rail Conference, Chicago, IL, April 22–24, 2003, American Society of Mechanical Engineers, United Engineering Center, 345 East 47th Street, New York, NY 10017, USA, 2003, pp. 149–159.
[39] F. Xia, H. True, The dynamics of the three-piece-freight truck, in: Proc. 18th IAVSD Symposium on Vehicle System Dynamics, The Dynamics of Vehicles on Roads and on Tracks, Taylor & Francis, London, UK, 2004, pp. 212–221.